VISIT…

Chapter 23

Thermohydrodynamic and Thermoelastohydrodynamic Lubrication

Symbols

A_c	slide/roll ratio, $2(u_b - u_a)/(u_b + u_a)$
a	distance, see Fig. 23.1, m
b	width of bearing, m
C_p	specific heat of material at constant pressure, J/(kg·°C)
D_x	diameter of contact ellipse along x axis, m
E	modulus of elasticity, Pa (or N/m^2)
E'	effective elastic modulus, $2\left(\frac{1-\nu_a^2}{E_a} + \frac{1-\nu_b^2}{E_b}\right)^{-1}$, Pa (or N/m^2)
F_{KE}	dimensionless kinetic energy parameter
F_{WK}	dimensionless flow work parameter
G	dimensionless materials parameter, $\xi E'$
H	dimensionless film thickness
H^*	used in Eq. (23.17)
H_p	dimensionless power dissipated by lubricant
h	film thickness, m
$\check{K}$	dimensionless interface conductivity parameter
K_f	lubricant thermal conductivity, W/(m·°C)
L	length of pad, m
ℓ	loading parameter
M	thermal loading parameter, see Eqs. (23.12) to (23.15)
N	thermal resistance ratio, see Eq. (23.5)
P	dimensionless pressure
p	pressure, Pa (N/m^2)
R	curvature radius, m
r	radius, m
S	network resistance, see Eqs. (23.1) to (23.4)
$\check{T}$	difference of dimensionless shear stresses
t_m	temperature, °C
$t_{m,o}$	ambient temperature, °C
U	dimensionless speed parameter, $\eta_0 \bar{u}/E' R_x$
u	velocity in x direction, m/s
$\bar{u}$	mean surface velocity in x direction, m/s

Copyright © 2004 Marcel Dekker, Inc.

W	dimensionless load parameter, $w_z'/E'R_x$
W^*	load parameter, see Eq. (23.16)
w	load, N
w_z	normal applied load, N
w_z'	normal applied load per unit width, N/m
X_r	dimensionless x coordinate for rectangular conjunctions
x, y, z	Cartesian coordinates, m
Z_1	viscosity-pressure index
α	temperature coefficient of viscosity
α_{k1}	piezothermal-conductivity constant of first kind, 1.73×10^{-9} m^2/N
α_{k2}	piezothermal-conductivity constant of second kind, 6.91×10^{-10} m^2/N
$\alpha_{\rho 1}$	piezodensity constant of first kind, 0.6×10^{-9} m^2/N
$\alpha_{\rho 2}$	piezodensity constant of second kind, 1.7×10^{-9} m^2/N
β_η	temperature-viscosity coefficient, K^{-1}
β_ρ	dimensionless thermodensity constant
γ^*	limiting-shear-strength proportionality constant
η	absolute viscosity, Pa·s (or N·s/m^2)
η_0	absolute viscosity at $p = 0$ and constant temperature, Pa·s (or N·s/m^2)
κ	thermal diffusivity
μ	coefficient of sliding friction
ν	Poisson's ratio
ξ	pressure-viscosity coefficient, m^2/N
ρ	density, kg/m^3
τ_L	limiting shear stress, Pa (or N/m^2)
$\hat{\tau}_L$	average dimensionless limiting shear strength across the film

Subscripts

a	solid a
b	solid b
c	combined conduction and convection
d	conduction
l	lubricant
p	pad
r	runner
v	convection

23.1 Thermohydrodynamic Lubrication

23.1.1 Introduction

Thermohydrodynamic lubrication (THL) treats the influence of temperature on the hydrodynamic lubrication process, especially its influence on rheological properties of the lubricant that affect the ability to generate films. Many researchers have addressed various aspects of THL problems for a wide variety of applications, so this chapter is intended to introduce key concepts. The interested reader is referred to the book by Pinkus (1990) or the review papers by Pinkus and Wilcock (1980) and Khonsari (1987) for a more in-depth treatment.

The first part of this chapter presents a framework for THL problems based on a lumped parameter approach that considers the wide variety of heat flow paths that are possible in lubrication problems. This allows a consideration of regimes wherein certain paths become negligible or dominant, and presents the results in a form similar to the bearing charts of Chapter 20. A major

Copyright © 2004 Marcel Dekker, Inc.

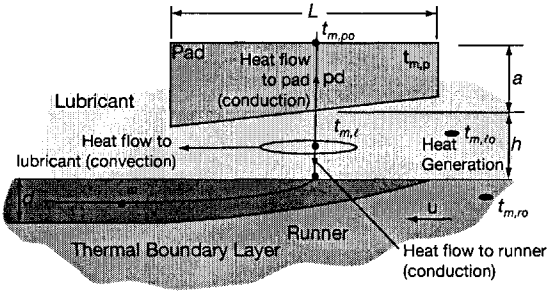

Figure 23.1: Heat flow paths in a slider bearing. [*From Wilson (1998)*].

contribution to this portion of the chapter comes from Wilson (1998).

23.1.2 Thermal Resistances

Recall from Chapter 20 that Johnson (1970) was able to consider the contribution of different effects to EHL and then construct charts describing this framework (Fig. 20.2). This framework has been extremely useful in understanding EHL numerical solutions and in applying them to practical problems. A recent paper by Wilson (1998) presents a similar useful framework for thermohydrodynamic lubrication, and is the basis for this section.

One of the main problems associated with THL problems is the multiplicity of heat transfer paths and modes of heat transfer. For example, consider the linear slider bearing of Fig. 23.1. Note that two heat flow paths have been neglected; convection across the film was shown by Dowson and Hudson (1964) to be unimportant compared to convection along the film. Similarly, conduction through the runner is neglected, since speeds that result in hydrodynamic films are usually large enough to make convection in the runner dominant. Further examination of these effects can be found in Carslaw and Jaeger (1959).

The main source of heat generation is viscous shear in the lubricant, as considered in the quasi-thermal analysis in Section 11.2. The main sources of heat loss from the system are through three paths, as illustrated in the equivalent resistances in Fig. 23.2. Note that each resistance is denoted by a variable with two subscripts; the first relates to the medium of heat transfer (lubricant, pad or runner); the second relates to the type of heat transfer (conduction, convection, or combined). Thus, heat that remains in the lubricant and carried away by convection would receive the indices lv; that removed through the pad by conduction receives pd, etc.

The resistances for the network in Fig. 23.2 have been given by Wilson (1998) as

$$S_{lv} = \frac{2}{\rho_l C_{pl} hub} \tag{23.1}$$

Copyright © 2004 Marcel Dekker, Inc.

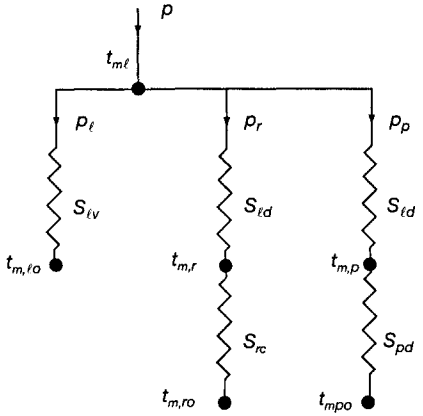

Figure 23.2: Equivalent resistance network for the bearing system of Fig. 23.1. [*From Wilson (1998)*].

$$S_{ld} = \frac{h}{2LbK_{fl}} \tag{23.2}$$

$$S_{pd} = \frac{a}{LbK_{fp}} \tag{23.3}$$

$$S_{rc} = \frac{1}{b\sqrt{uLK_{fr}\rho_r C_{pr}}} \tag{23.4}$$

where

ρ_l = lubricant density, kg/m^3
C_p = specific heat, J/(kg·°C)
h = film thickness, m
u = runner speed, m/s
b = bearing width, m
L = pad length, m
K_f = thermal conductivity, W/(m·°C)

and the subscripts l, r, and p refer to the lubricant, runner, and pad, respectively.

23.1.3 Thermal Loading Parameters and Their Relative Importance

It is important to judge the relative importance of different modes of heat transfer in order to ascertain under what conditions one or more paths can be neglected in analysis. A nondimensional measure $N_{ij/lm}$ can be defined to judge the importance of mode ij compared to mode lm. Since the importance of a heat transfer mechanism is inversely proportional to its thermal resistance, we can write

$$N_{ij/mn} \propto \frac{S_{mn}}{S_{ij}} \tag{23.5}$$

Copyright © 2004 Marcel Dekker, Inc.

The results are summarized in Table 23.1. As an example, consider the relative importance of convective heat transfer and conduction across the film in the lubricant. This is given by

$$N_{lv/ld} = \frac{uh^2\rho_l C_{pl}}{LK_{fl}} = \frac{uL}{\kappa_l}\left(\frac{h}{L}\right)^2 \tag{23.6}$$

where κ_l is the thermal diffusivity for the lubricant. Note that the right side of Eq. (23.6) is the Peclet number weighted by the quantity $(h/L)^2$ to compensate for thin film geometry.

The measures shown in Table 23.1 are useful for simplifying the THL problem in many cases. For example, the parameter $N_{lv/ld}$ given in Eq. (23.6) is already known as an important parameter in THL. If $N_{lv/ld}$ is large, then heat is retained in the lubricant and removed through convection. If $N_{lv/ld}$ is small, then heat is conducted to the adjacent surfaces. If $N_{lv/ld}$ is around unity, then a full numerical solution is required.

In THL, it is important to understand the change in lubricant film formation capability associated with a change in temperature. This can be accomplished by defining nondimensional loading parameters:

$$\ell_{ij} = \alpha p_0 S_{ij}$$

where α is the temperature coefficient of viscosity at some temperature defined by

$$\alpha = \frac{1}{\eta}\frac{d\eta}{dt_m}$$

and H_p is the isothermal viscous power defined by

$$H_p = \frac{\eta_0 \bar{u}^2 Lb}{h}$$

Wilson (1998) derives the nondimensional loading parameters as

$$\ell_{lv} = \frac{\alpha\eta_0\bar{u}L}{\rho_l C_{pl}h^2} \tag{23.7}$$

$$\ell_{ld} = \frac{\alpha\eta_0\bar{u}^2}{K_{fl}} \tag{23.8}$$

$$\ell_{pd} = \frac{\alpha\eta_0\bar{u}^2 a}{hK_{fp}} \tag{23.9}$$

$$\ell_{rc} = \frac{\alpha\eta_0\bar{u}^{3/2}L^{1/2}}{h\sqrt{K_{fr}\rho_r C_{pr}}} \tag{23.10}$$

Some of these parameters are well known, others less so. ℓ_{lv} is important in the analysis of bearings where convective heat transfer by lubricant is more important than conduction. This is referred to as the "first thermal parameter"

Copyright © 2004 Marcel Dekker, Inc.

Table 23.1: Measures $N_{ij/mn}$ of relative importance of cooling mechanisms. [*From Wilson (1999).*]

Denominator suffixes (mn)	Numerator suffixes (ij)			
	lv	ld	pd	rc
lv	1	$\frac{LK_{fl}}{uh^2\rho_l C_{pl}}$	$\frac{LK_{fp}}{uah\rho_l C_{pl}}$	$\frac{L^{1/2}\sqrt{K_{fr}\rho_r C_{pr}}}{u^{1/2}h\rho_l C_{pl}}$
ld	$\frac{uh^2\rho_l C_{pl}}{LK_{fl}}$	1	$\frac{hK_{fp}}{aK_{fl}}$	$\frac{u^{1/2}h\sqrt{K_{fr}\rho_r C_{pr}}}{L^{1/2}K_{fl}}$
pd	$\frac{uah\rho_l C_{pl}}{LK_{fp}}$	$\frac{aK_{fl}}{hK_{fp}}$	1	$\frac{u^{1/2}a\sqrt{K_{fr}\rho_r C_{pr}}}{K_{fp}}$
rc	$\frac{u^{1/2}h\rho_l C_{pl}}{L^{1/2}\sqrt{K_{fr}\rho_r C_{pr}}}$	$\frac{L^{1/2}K_{fl}}{u^{1/2}h\sqrt{K_{fr}\rho_r C_{pr}}}$	$\frac{K_{fp}}{u^{1/2}a\sqrt{K_{fr}\rho_r C_{pr}}}$	1

Copyright © 2004 Marcel Dekker, Inc.

by Fillon and Khonsari (1996) and the "adiabatic constant" by Pinkus (1990). ℓ_{ld} is important when conduction by the lubricant is more important than convection, which is the case in many EHL problems (Cheng 1967) as well as metal forming problems (Wilson and Mahdavian 1974). Fillon and Khonsari refer to ℓ_{ld} as the "second thermal parameter." The other parameters are more obscure.

For isothermal problems, the load and the film thickness are related by

$$w = \frac{c_p \eta_0 \bar{u} L^2 b}{h^2} \tag{23.11}$$

where c_p is a constant that depends on the geometry. Eq. (23.11) can be used to eliminate h from Eqs. (23.7) through (23.10) to obtain a new set of thermal loading problems given by

$$M_{lv} = \frac{\alpha w}{\rho_l C_{pl} L b} = \frac{\alpha \bar{p}}{\rho_l C_{pl}} \tag{23.12}$$

$$M_{ld} = \frac{\alpha \eta_0 \bar{u}^2}{K_{fl}} \tag{23.13}$$

$$M_{pd} = \frac{\alpha \eta_0^{1/2} \bar{u}^{3/2} a w^{1/2}}{K_{fp} L b^{1/2}} \tag{23.14}$$

$$M_{rc} = \frac{\alpha \eta_0^{1/2} \bar{u} w^{1/2}}{\sqrt{(Lb) K_{fr} \rho_r C_{pr}}} \tag{23.15}$$

where the geometry constant c_p has been ignored.

23.1.4 Thermal Hydrodynamic Lubrication Regimes

Wilson (1998) showed that the following equations give the effect of temperature on film thickness and load:

$$\ln w^* = -\frac{2 w^* L_{ld} L_{lv}}{L_{ld} + 4 L_{lv}} \tag{23.16}$$

$$\ln H^* = -\frac{2 \left(H^*\right)^2 M_{ld} M_{lv}}{c_p \left(H^*\right)^2 M_{ld} + 2 M_{lv}} \tag{23.17}$$

Figure 23.3 shows the results of Eq. (23.16) as a function of thermal loading parameters ℓ_{ld} and ℓ_{lv}. The plot has also been subdivided by dashed lines to show the different regimes of THL. The isothermal line has been drawn where the reduction in load support is less than 5% ($w^* > 0.95$). At small values of ℓ_{ld} and ℓ_{lv}, the problem is isothermal. Increases in either ℓ_{ld} or ℓ_{lv} generally reduces the load support.

Figure 23.4 shows the effect of thermal loading parameters M_{ld} and M_{lv} on the film thickness obtained from Eq. (23.17). Comparing Figs. 23.3 and

Copyright © 2004 Marcel Dekker, Inc.

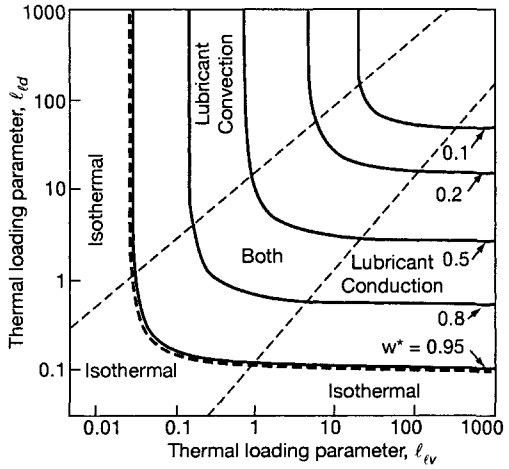

Figure 23.3: Regimes of thermohydrodynamic lubrication using nondimensional load w^* and ℓ_{ij} parameters. [*From Wilson (1998)*].

23.4, it should be noted that M_{lv} has a larger effect on film thickness than M_{ld}, whereas ℓ_{ld} and ℓ_{lv} have roughly the same effect on load support. This can be seen by the rough symmetry in Fig. 23.3 and the smaller horizontal spacing of film thickness contours for large M_{ld} in Fig. 23.4.

It is interesting to compare Fig. 23.4 with Fig. 23.2. Figure 23.2 has film thickness contours that are greater than unity, whereas Fig. 23.4 has contours that are less than unity. This represents a fundamental difference between EHL and THL problems: EHL effects tend to increase film thickness, while THL effects reduce film thickness.

The loading parameters ℓ_{ij} and M_{ij} are extremely useful for determining the important physical effects, and it would be beneficial to designers if researches used this framework in the presentation of numerical results.

23.2 Thermoelastohydrodynamic Lubrication

23.2.1 Introduction

An example of a complete solution is then obtained in this chapter for elastohydrodynamically lubricated conjunctions in line contacts when the effects of temperature and the non-Newtonian characteristics of lubricants with limiting shear strength are considered. The fast approach developed in Chapter 18 is used to solve the thermal Reynolds equation by using the complete circular non-Newtonian fluid model and considering both velocity and stress boundary conditions. The reason and the occasion for incorporating stress boundary conditions in the circular model are discussed. A conservative form of the energy equation is developed by using the finite control volume approach. Analytical solutions for solid surface temperatures that take into consideration

Copyright © 2004 Marcel Dekker, Inc.

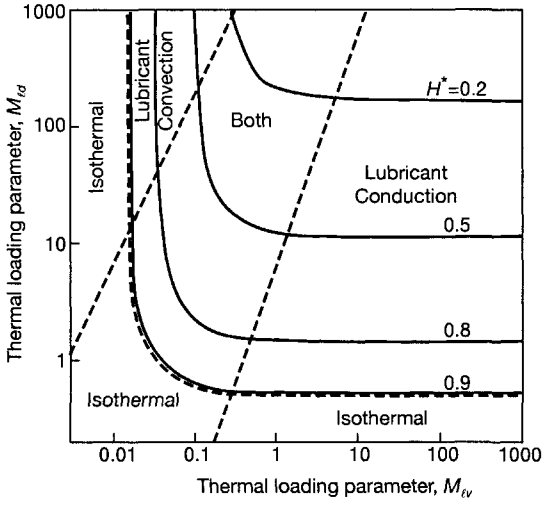

Figure 23.4: Regimes of thermohydrodynamic lubrication using M_{ij} parameters. [*From Wilson (1998)*].

two-dimensional heat flow within the solids are used. A straightforward finite difference method called "successive overrelaxation by lines" is employed to solve the energy equation. Results of thermal effects on film shape, pressure profile, streamlines, and friction coefficient are presented.

Lubrication analysis that uses isothermal Newtonian fluid models has been well developed. The film shape and the pressure distribution have been reasonably well predicted. However, the traction could not be anticipated correctly. The need to incorporate the thermal effect, the non-Newtonian effect, or both was recognized long ago (e.g., by Cheng, 1965). Since then, many numerical analyses that considered either thermal effects on EHL with Newtonian lubricants or the effects of non-Newtonian lubricants on isothermal EHL conjunctions have been performed (e.g., by Dowson and Whitaker, 1965-1966; Zhu and Wen. 1984; Ghosh and Hamrock, 1985; Sadeghi and Dow, 1987; and Lee and Hamrock, 1990). Some preliminary studies on both the effects of temperature rises and the characteristics of non-Newtonian fluids were conducted with various levels of numerical convergence difficulty (e.g., by Conry, 1981; Wang and Zhang, 1987; and Wang et al., 1991). With the discovery of the limiting shear strength of lubricants by Smith (1958, 1959), different rheological models have been proposed to characterize the behavior of the non-Newtonian fluids with limiting shear strength by Jacobson (1070), Gecim and Winer (1980) and Lee and Hamrock (1990).

The traditional thermal EHL models used the nonconservative form of the energy equation. This is believed to be the major cause of the difficulty in solving the numerical convergence problem that has been encountered, for example, by Cheng (1967), Conry (1981), Zhu and Wen (1984), and Wang et al. (1991). It meant that some delicate numerical procedures needed to be implemented to

Copyright © 2004 Marcel Dekker, Inc.

obtain a converged solution, especially when the reverse-flow zones were analyzed. The work presented in this chapter represents a conservative form of the energy equation that was solved by using a straightforward scheme of successive overrelaxation by lines, a popular finite difference method. No extra effort is needed to obtain a convergence solution for the entire conjunction including the inlet, Hertzian contact, and outlet zones.

23.2.2 Theoretical and Numerical Schemes

In solving the Reynolds equation for EHL problems, Okamura (1982) introduced the Newton-Raphson scheme to solve the highly nonlinear system equation. Houpert and Hamrock (1986) successfully developed a systematic approach for solving the elastic deformation and Reynolds equations simultaneously. This is the well-known "fast approach" covered in Chapter 19. Lee and Hamrock (1990) improved the fast approach by solving for the outlet location instead of the dimensionless flow rate as one of the system unknowns. This improvement further automated the fast approach. In deriving the Jacobian factors for the new system unknown, however, Lee and Hamrock neglected the effect of pressure distribution on the deformation at the exit. This is amended in Hsiao and Hamrock (1992) and in this chapter to fully expedite the solution scheme.

Lee and Hamrock (1990) have successfully used the circular model in analyzing isothermal EHL problems. Their work established the general procedure of using the circular model. However, its implementation was not completed in two senses. First, the derivation of the Jacobian factors was not complete, especially the effects of the non-Newtonian viscosity variable on the dimensionless offset film thickness, one of the system unknowns. This incompleteness slowed down the convergence of the calculation and probably prevented a completely convergent solution. The formulation presented in this chapter as well as in Hsiao and Hamrock (1992) gives the derivation of the Jacobian factors and eliminates the potential difficulty of convergence. Second, as mentioned by Wilson and Huang (1990), stress boundary conditions may have to be substituted for the velocity boundary condition to continue the computation and obtain a converged solution. However, in contradiction to Wilson and Huang, the need to switch boundary conditions is not due to the circular model theory but to the inexact representation of a real number by a digital computer. When the product of the viscosity and the shear strain rate is greater than a certain amount, the value of the boundary shear stress calculated by the digital computer may reach or exceed the limiting shear strength even though the theoretical value of the shear stress is still less than the limiting shear strength. Numerical procedures are developed in the current work to remedy this shortcoming of digital computation.

Interest in film collapse in an EHL conjunction was raised by Shieh and Hamrock (1991). How temperature rises in the flow field affect film collapse has been pondered since then. This chapter attempts to answer this question. A major contribution to this chapter comes from Hsiao and Hamrock (1992).

Copyright © 2004 Marcel Dekker, Inc.

In solving a thermal EHL problem, two systems of equations that depend on each other must be solved (i.e., the thermal Reynolds equation and the energy equation). The coupling of these two systems of equations results from the pressure-temperature dependence of the lubricant properties. The resultant film thickness of the conjunction involves the elastic deformation of the bounding solids. The elastic deformation and the field pressure also depend on each other. A systematic approach has been developed by Houpert and Hamrock (1986) for solving for the elastic deformation and the field pressure simultaneously (see Chapter 21). The use of an asymptotic limiting-shear-stress model such as the circular model occasionally requires imposing various stress boundary conditions. Different Reynolds equations result from this consideration. Moreover, the resultant field temperature and the surface temperature of the bounding solids also depend on each other. A systematic approach developed by Hsiao and Hamrock (1992) is used in this chapter to solve for the field temperature and the temperatures of the solid surfaces simultaneously. The following sections summarize the use of equations for the lubricant properties, the development of the thermal Reynolds equations that consider various boundary conditions, the derivation of a conservative form of the energy equation with a two-dimensional heat flow model for calculating solid surface temperatures, and the evolution of the systematic approach that solves for the field temperature and the surface temperature simultaneously. The numerical methods used to solve the individual equations and the coupling of the systems of equations are also described.

23.2.3 Outline of Approach

The circular non-Newtonian fluid model introduced by Lee and Hamrock (1990) and covered in Chapter 4 is used as the basic rheology model in the thermal EHL analysis results presented here. Some of the key components of the analysis are the following:

1. The properties of any existing lubricant vary with pressure and temperature, some weakly, some strongly. Continuous functions are favored to describe these relationships in numerical models that simulate lubricant behavior.

2. Line contact is assumed (i.e., side leakage is neglected).

3. The film thickness is much smaller than the equivalent radius of the contact. This may further imply

   (a) That the pressure gradient across the film thickness is negligible (that is, $\partial p/\partial z = 0$)

   (b) That the velocity component in the z direction, which is the direction across the film thickness, is much smaller than that in the x direction, which is the main-stream direction (that is, $w \ll u$ and then $\partial w/\partial x \ll \partial u/\partial z$)

Copyright © 2004 Marcel Dekker, Inc.

(c) That the shear stress acting on the yz plane is negligible

4. The inertia effect is negligible relative to the viscous effect.

5. The fluid flow and the heat flow are in steady state within the lubricant body.

6. The inlet conditions are ambient (i.e., the temperature is the given ambient temperature and the pressure is the zero gage pressure).

7. The pressure at the exit is the Reynolds boundary pressure (i.e., the pressure is the zero gage pressure and the gradient of the pressure is zero also). The thermal condition is adiabatic (and ambient) at a location infinitely far away from the exit. Practically, it is assumed to be adiabatic at the outlet, a location with a finite distance away from the exit.

8. The solid surface temperatures are calculated for the moving distributed heat sources that are generated by the temperature gradients of the lubricant adjacent to the liquid-solid interfaces. Only the start transient period is taken into account in lieu of the heat sink characteristic of the fluid beyond the outlet. The frictional heat generated at the liquid-solid interfaces is considered when the stress boundary condition is imposed.

9. The numerical scheme is described by Hsiao and Hamrock (1992), including derivation of all components of the Jacobian matrix to obtain fast and complete convergence of solutions.

Lee and Hamrock (1990) and Hamrock (1994) summarize the key rheological equations.

23.2.4 Results and Discussion

Two series of computations, referred to as the "case-1" and "case-2" series, have operating conditions listed in Tables 23.2 to 23.5. Table 23.2 shows the dimensional operating factors. Table 23.3 gives the properties of the bounding solids. The properties of the lubricants at ambient and atmospheric conditions are summarized in Table 23.4, while the pressure-temperature influencing factors on the properties of the lubricants are shown in Table 23.5. In addition, Table 23.6 gives the dimensionless operating parameters.

Note that case-2 series uses operating parameters identical to those that Shieh and Hamrock (1991) used in their isothermal study of non-Newtonian effects on film collapse. Using these parameters allows direct comparison between the thermal and isothermal results. The case-1 series uses operating parameters identical to those that Lee and Hamrock (1990) used in their study of circular non-Newtonian behavior in EHL conjunctions, in which the reach of the limiting shear strength at a low slide/roll ratio was encountered. This series of calculations demonstrates the numerical behavior of the asymptotically

Copyright © 2004 Marcel Dekker, Inc.

Table 23.2: Operating parameters for two cases.

Parameters	Case 1	Case 2
Mean surface velocity in x-direction $\tilde{u}$, m/s	0.59634	1.84843
Load per unit width w', N/m	0.147×10^6	0.147×10^6
Radius of curvature sum R, m	0.01114	0.01114
Ambient temperature $t_{m,0}$, °C	40	40

Table 23.3: Properties of bounding solids.

Effective elastic modulus E', Pa	2.2×10^{11}
Density of solids ρ_a and ρ_b, kg/m^3	7850
Thermal conductivity of solids K_{fa} and K_{fb}, W/(m·K)	52
Specific heat of solids $C_{p,a}$ and $C_{p,b}$, J/(kg·K)	460

approached limiting-shear-strength model and shows the computational scheme that makes the convergent solution achievable.

Figures 23.5 to 23.11 give the results of case-2 computations. Figures 23.5a to c shows the three-dimensional temperature distributions for slide/roll ratios A_c of 1, 2, and 10. The temperature rises in the inlet zone are generally negligible relative to those in the Hertzian zone. In cases of pure rolling the maximum temperature rise in the whole conjunction is less than 1°C. The temperature distribution is completely flat in a scale such as that used in Fig. 23.5 and therefore is not shown. At low slide/roll ratios (that is, $A_c \leq 2$) the temperature distribution in the entire inlet zone is also flat. At greater slide/roll ratios, at which the solid surfaces are moving in opposite directions, the convective flows raise the downstream temperatures while maintaining low temperatures upstream in both the inlet and outlet zones.

Figure 23.6 gives a closer look at the temperature profiles at the lower solid-liquid interface ($Z = 0$), the midfilm ($Z = 0.5$), and the upper solid-liquid interface ($Z = 1$). It shows that at a lower slide/roll ratio (Fig. 23.6a) the temperature difference between the central film and the solid-liquid boundaries, as well as the magnitude of the temperature rises, is less than that at a higher slide/roll ratio. At low slide/roll ratios the midfilm temperature is higher than the solid surface temperatures in both the inlet and Hertzian contact zones, whereas at slide/roll ratios higher than 2 it is higher only at the central part of the Hertzian contact zone.

Comparing Fig. 23.7b with Fig. 23.7a, which duplicates the results of Shieh and Hamrock (1991), shows the thermal effects on the formation of film shape, pressure profile, and streamlines at a slide/roll ratio of 10. With temperature effects not considered, Fig. 23.7a predicts the possibility of film collapse in an EHL conjunction lubricated with a non-Newtonian lubricant and operated

Copyright © 2004 Marcel Dekker, Inc.

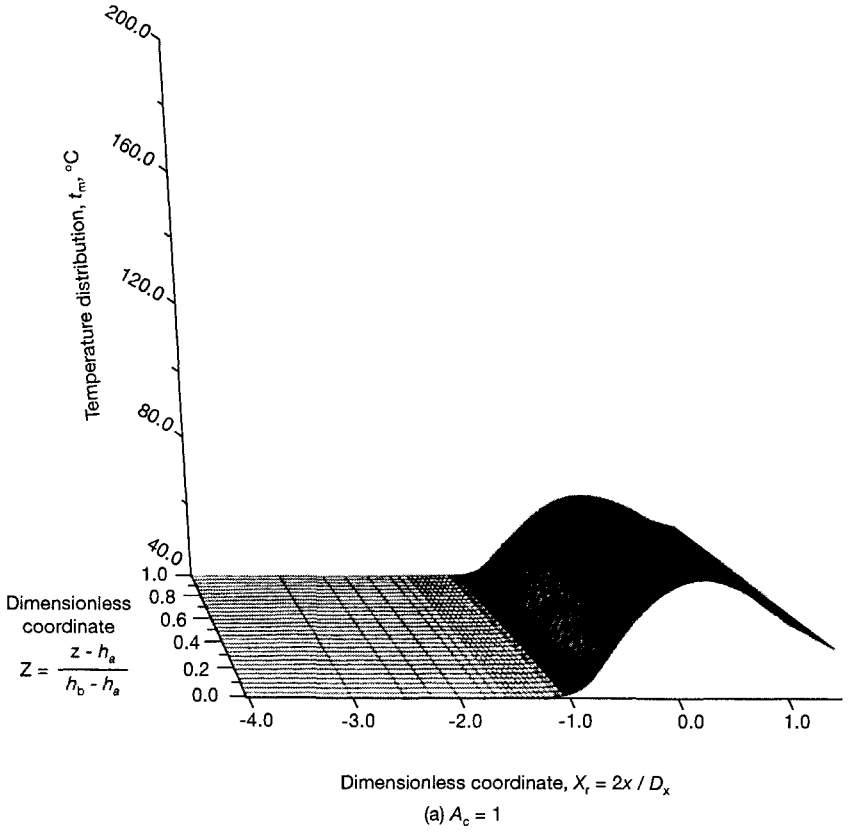

Figure 23.5: Temperature distribution for case 2 at various slide/roll ratios: (a) A_c =1, (b) $A_c = 2$, and (c) A_c =10. [*From Hsiao and Hamrock (1992).*]

Copyright © 2004 Marcel Dekker, Inc.

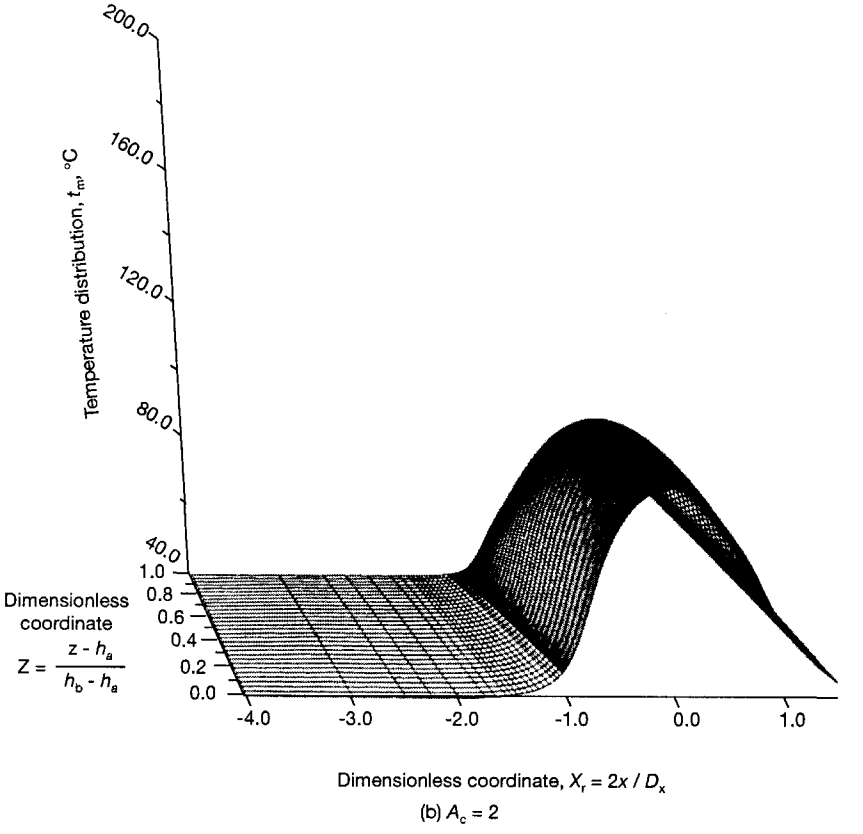

Figure 23.5: *Continued.*

Copyright © 2004 Marcel Dekker, Inc.

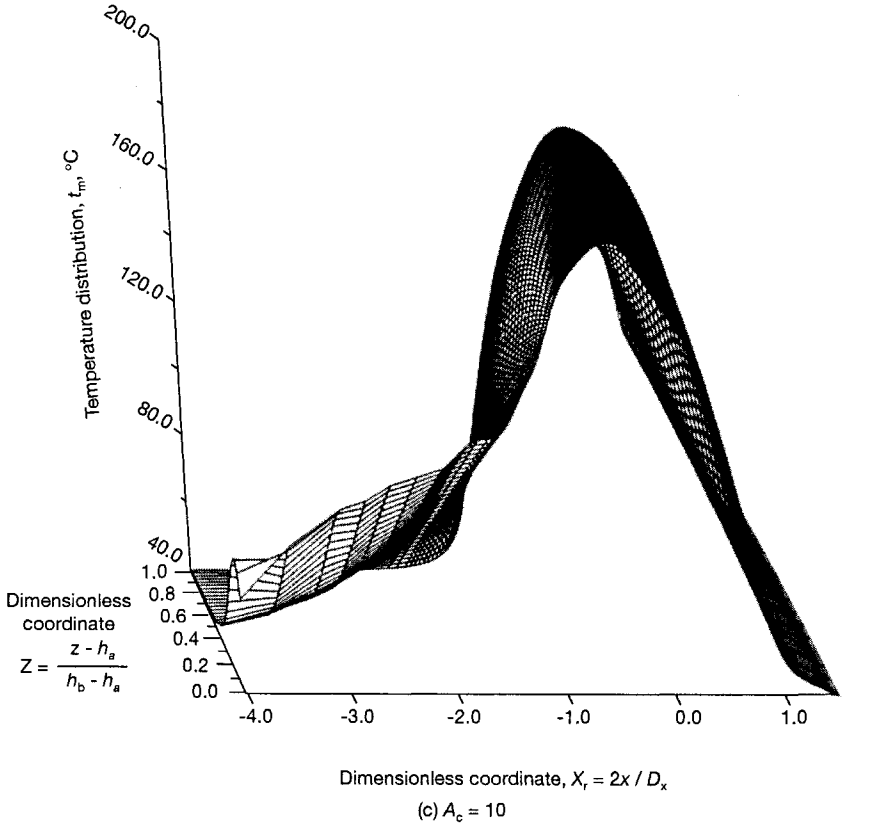

Figure 23.5: *Concluded.*

Copyright © 2004 Marcel Dekker, Inc.

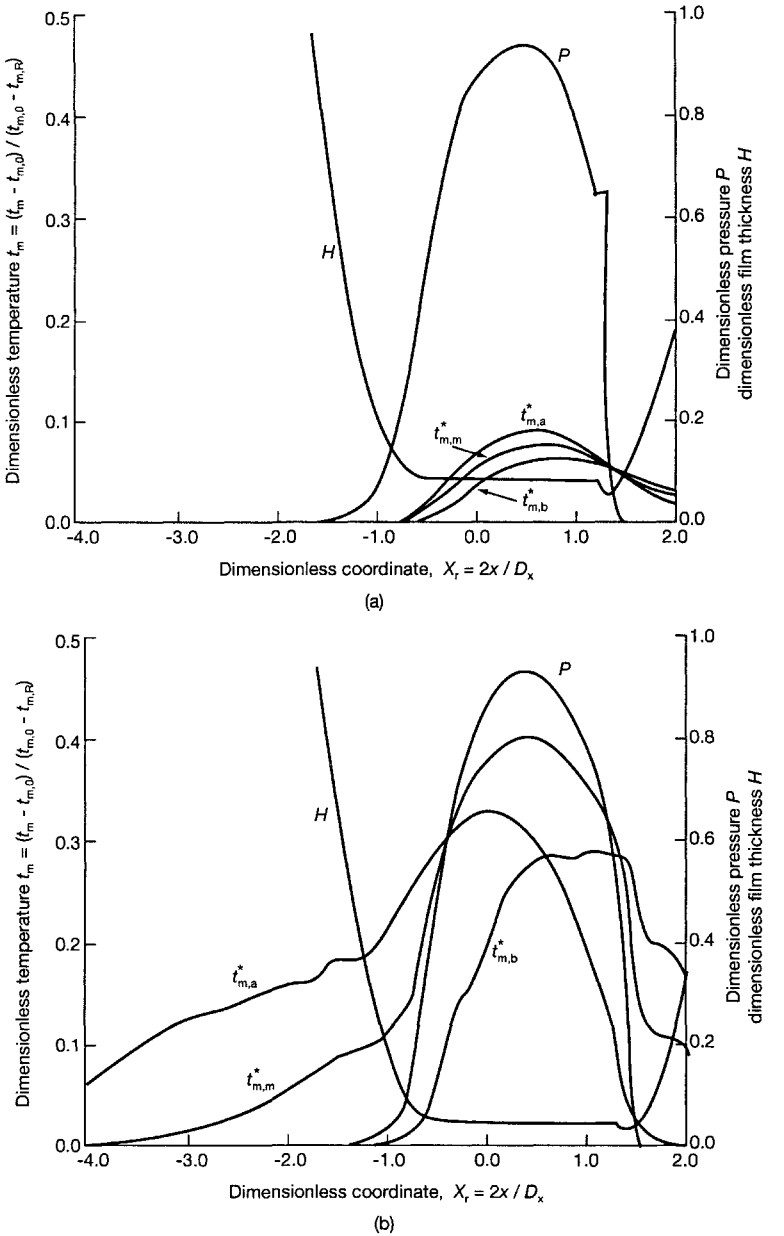

Figure 23.6: Surface and midfilm dimensionless temperatures as well as the film shape and pressure for case 2 and slide/roll ratios of (a) $A_c = 1.0$ and (b) $A_c = 10$. [*From Hsiao and Hamrock (1992).*]

Copyright © 2004 Marcel Dekker, Inc.

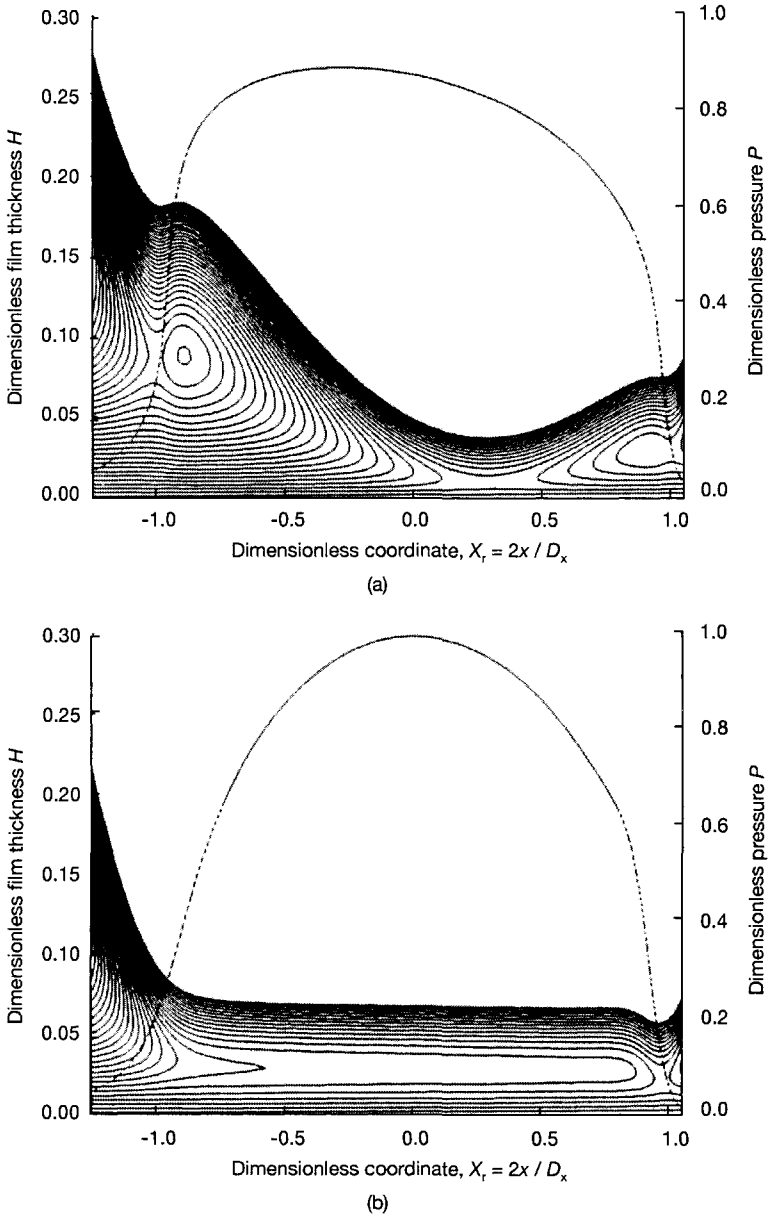

Figure 23.7: Streamlines as well as film shape and pressure profiles for case 2 at a slide/roll ratio of 10. (a) Isothermal results; (b) thermal results. [*From Hsiao and Hamrock (1992).*]

Copyright © 2004 Marcel Dekker, Inc.

Table 23.4: Ambient-atmosphere properties of lubricant

Property	Case 1	Case 2
Density of lubricant at atmospheric conditions ρ_o, kg/m^3	866	866
Thermal conductivity of lubricant at atmospheric conditions $K_{f,0}$, W/(m·K)	0.124	0.124
Specific heat of lubricant at atmospheric conditions $C_{p,0}$, J/(kg·K)	2000	2000
Absolute viscosity at $p = 0$ and $t_m = 40°C$, η_0, Pa·s	0.04110	0.01326
Limiting shear strength at $p = 0$ and $t_m = 40°C$, τ_L, Pa·s	1.98×10^7	1.98×10^7

at an extremely high slide/roll ratio. However. Fig. 23.7b shows that the temperature rises in the flow field prevent a sharp decrease in film thickness near the center of the Hertzian contact zone. Furthermore, the pressure profile seems to be more Hertzian. It implies that at extremely high slide/roll ratios, two separate lubricant flows moving in opposite directions, instead of metal-to-metal contact, may develop in the Hertzian contact zone.

Figure 23.8 shows the viscosity profiles at slide/roll ratios of 0, 1, 2, and 10 for isothermal and thermal results. The viscosity profiles from the isothermal analysis reflect pressure distributions such as that shown in Fig. 23.7a. It also shows that the viscosity profiles remain almost unchanged when the bounding solid surfaces move in the same direction or one of the surfaces is stationary. When the bounding surfaces start to move in opposite directions, the magnitude of viscosity (influenced by pressure) clearly decreases, and the center of viscosity (pressure) shifts toward the starting point of the Hertzian contact zone.

On the other hand, the viscosity profiles from the thermal analysis indicate the synergistic effects of pressure and temperature. The decrease in viscosity with increasing slide/roll ratio is continuous and dramatic. The centers of these profiles remain almost unchanged. This lack of change reflects the fact that the pressure profiles are more Hertzian and that the temperature profiles follow more or less the same shape as the pressure profiles in the Hertzian contact zone.

The profiles in $\check{T}$, the difference of dimensionless boundary shear stresses, for various slide/roll ratios from isothermal and thermal analyses are given in Fig. 23.9. The profile of $\check{T}$ depicts the film shape and the slope of the pressure profile as can be seen in the definition of the stress difference, $\check{T} = \bar{\tau}_b - \bar{\tau}_a = 2WH(dP/dX)/\pi\check{\tau}_L$.

From the results of isothermal analyses the profiles of stress differences remain almost the same at slide/roll ratios less than 2. As the slide/roll ratio becomes larger, the stress difference becomes greater at the starting point and

Copyright © 2004 Marcel Dekker, Inc.

Table 23.5: Pressure-temperature influence factors on properties of lubricant

Factor	Case 1	Case 2
Viscosity-pressure index Z_1, dimensionless	0.689	0.580
Pressure-viscosity coefficient ξ, m^2/N	2.276×10^{-8}	1.582×10^{-8}
Viscosity-temperature index s_0, dimensionless	1.5	1.5
Temperature-viscosity coefficient β_η, 1/K	0.0216	0.0162
Limiting-shear-strength proportionality constant γ^*, Pa^{-1}	0.036	0.078
Temperature-limiting shear-strength coefficient $\beta_{\tau L}$, 1/K	585	585
Piezodensity constant, first kind, $\alpha_{\rho,2}$ m^2/N	0.6×10^{-9}	0.6×10^{-9}
Piezodensity constant, second kind, $\alpha_{\rho,2}$ m^2/N	1.7×10^{-9}	1.7×10^{-9}
Thermodensity constant β_ρ, dimensionless	6.5×10^{-4}	6.5×10^{-4}
Piezothermal-conductivity constant, first kind, $\alpha_{k,1}$, m^2/N	1.73×10^{-9}	1.73×10^{-9}
Piezothermal-conductivity constant, second kind, $\alpha_{k,2}$, m^2/N	6.91×10^{-10}	6.91×10^{-10}

less at the exit location of the Hertzian contact zone, with the peaks shifting toward the ends. The isothermal analysis confirms the formation of nips in the film thickness profile, as shown in Fig. 23.7a. It is believed that the double nips near the two ends create the circulating subflows within the Hertzian contact zone and prevent the lubricant from flowing through the conjunction.

However, the increase in stress differences at the starting point of the Hertzian contact zone means that more shear energy is created in this region. The increased shear energy increases the temperature by a significant amount and decreases the viscosity. The decrease in viscosity in turn decreases the pressure buildup. It may also prevent the formation of the nip in this region and allow more fluid to flow through the conjunction, as Fig. 23.7b shows.

Table 23.6: Dimensionless operating parameters.

Parameter	Case 1	Case 2
Speed parameter U	1.0×10^{-11}	1.0×10^{-11}
Load parameter W	6.0×10^{-5}	6.0×10^{-5}
Materials parameter G	5007	3480
Peclet number of lubricant P_{ef}	1147	3555
Kinetic energy parameter F_{KE}	0.652×10^{-3}	19.41×10^{-3}
Flow work parameter F_{WK}	0.466×10^{6}	1.433×10^{6}
Interface conductivity parameter $\check{K}_a$ and $\check{K}_b$	0.01535	0.01535

Copyright © 2004 Marcel Dekker, Inc.

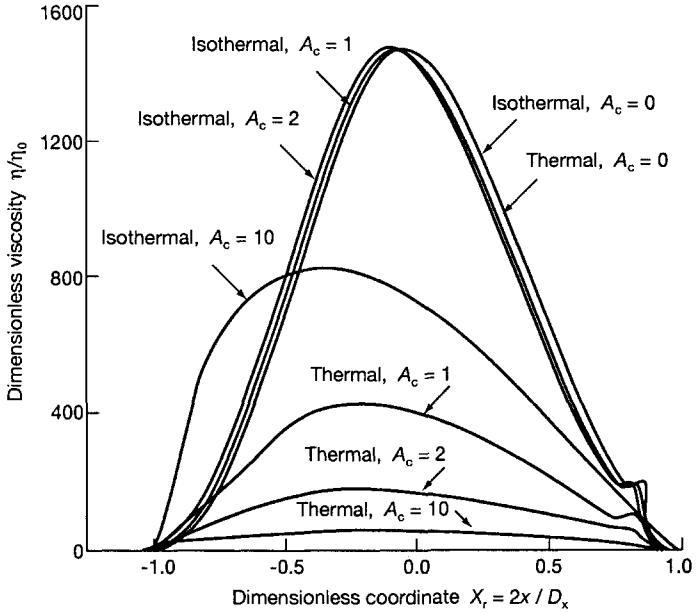

Figure 23.8: Viscosity profiles for case 2 at various slide/roll ratios for isothermal and thermal results. [*From Hsiao and Hamrock (1992).*]

One of the major objectives of the tribologist is to investigate the effects of both temperature and non-Newtonian characteristics on the traction generated in an EHL conjunction. Figure 23.10 gives one of the results, showing that the friction coefficient may be only one-half of that predicted by an isothermal non-Newtonian analysis for a high-slide-roll-ratio EHL conjunction if the temperature effect is considered.

Figure 23.11 shows the results of case-1 simulations. Figure 23.11a exhibits the three-dimensional temperature distribution at a slide/roll ratio of 0.1. Figure 23.11b records the distribution of stress boundaries at which the local limiting shear strength is imposed. Zone 1 used in Fig. 23.11b is the ordinary flow zone with velocity boundaries. Zone 2 is the flow zone with the limiting shear strength reached at the surface of solid a. Zone 3 is the flow zone with the limiting shear strength reached at the surface of solid *b*.

Figure 23.11c details the temperature profiles at the solid-liquid interfaces and the midfilm and shows the film shape and the pressure profile. Temperature spikes follow the pressure spike in the results of case-1 simulations, as depicted in Figs. 23.11a and c. The causes of these temperatures spikes are not well understood, but the fluctuation of the boundary shear stress differences in these

Copyright © 2004 Marcel Dekker, Inc.

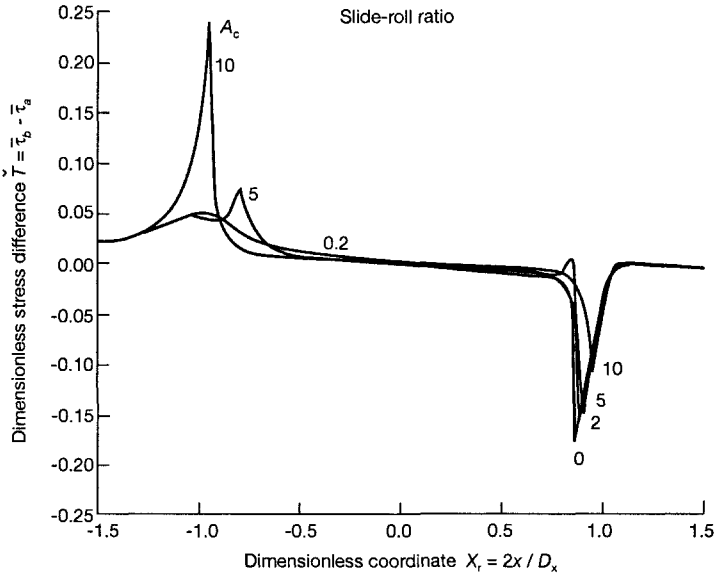

(a)

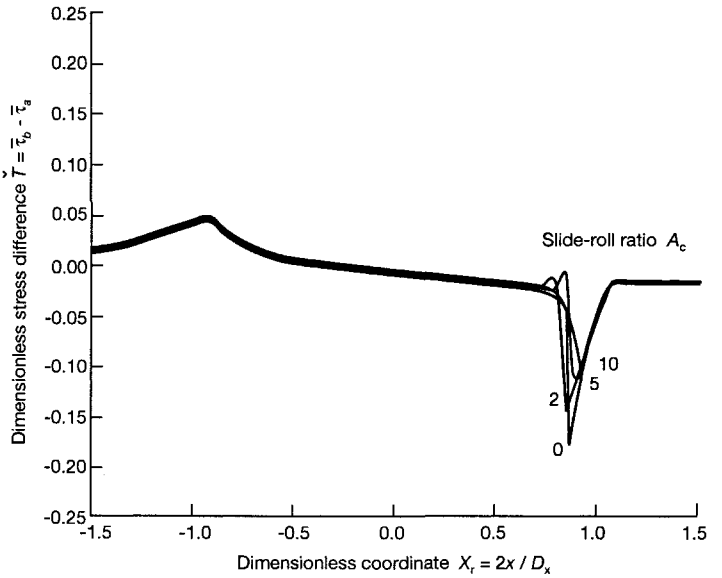

(b)

Figure 23.9: Stress-difference profiles for case 2 for various slide/roll ratios. (a) Isothermal results; (b) thermal results. [*From Hsiao and Hamrock (1992).*]

Copyright © 2004 Marcel Dekker, Inc.

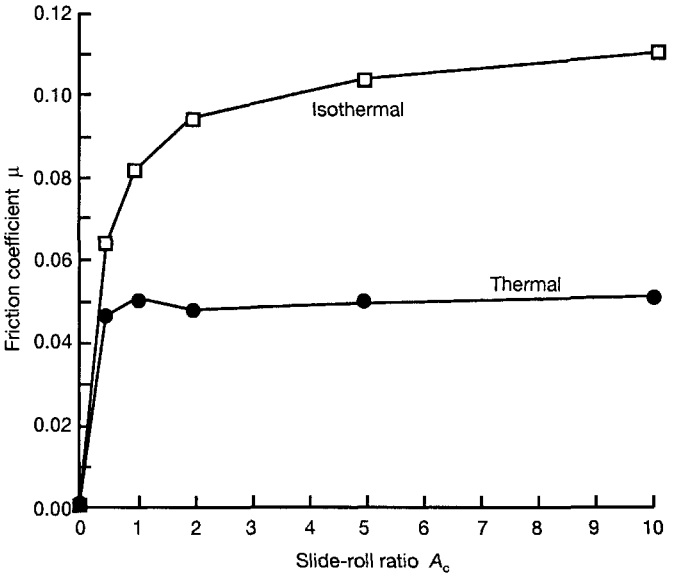

Figure 23.10: Effect of friction coefficient on slide/roll ratios for isothermal and thermal considerations. [*From Hsiao and Hamrock (1992).*]

regions may explain them [Fig. 23.11d]. That is, when the stress difference sharply increases or decreases, the temperature increases or decreases in the same manner.

23.3 Closure

In this chapter the fast approach was completed and used to solve the thermal Reynolds equations for EHL conjunctions with circular non-Newtonian fluids. It fully automates and expedites the solution scheme.

The use of fictitious Reynolds equations ensured the validity of the solutions obtained and helped identify the flow zones with the boundary shear stresses that reached the local limiting shear strength of the lubricant. Imposing shear-stress boundary conditions enabled the simulation of an EHL conjunction lubricated by a circular non-Newtonian lubricant when the limiting shear strength of the lubricant is reached.

Using the thermal influence coefficients and embedding the solid-liquid interface temperatures into the discrete energy equations enabled the application of a straightforward successive-overrelaxation-by-lines finite difference method. This method solved for the field temperatures and the interface temperatures

Copyright © 2004 Marcel Dekker, Inc.

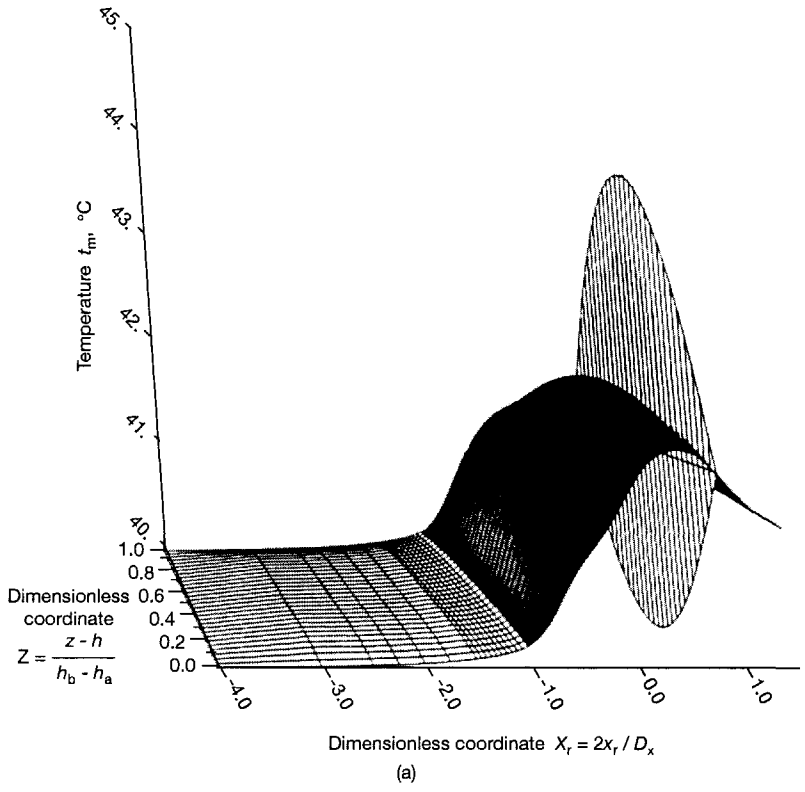

Figure 23.11: Results for case 1 at slide/roll ratio of 0.1. (a) Temperature distribution; (b) velocity contours indicating flow distribution; (c) surface and midfilm temperature as well as film thickness and pressure; (d) stress difference profile. [*From Hsiao and Hamrock (1992).*]

Copyright © 2004 Marcel Dekker, Inc.

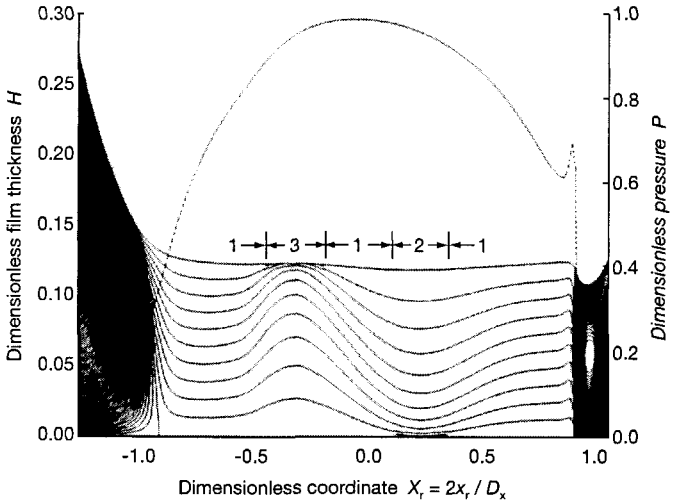

(b)

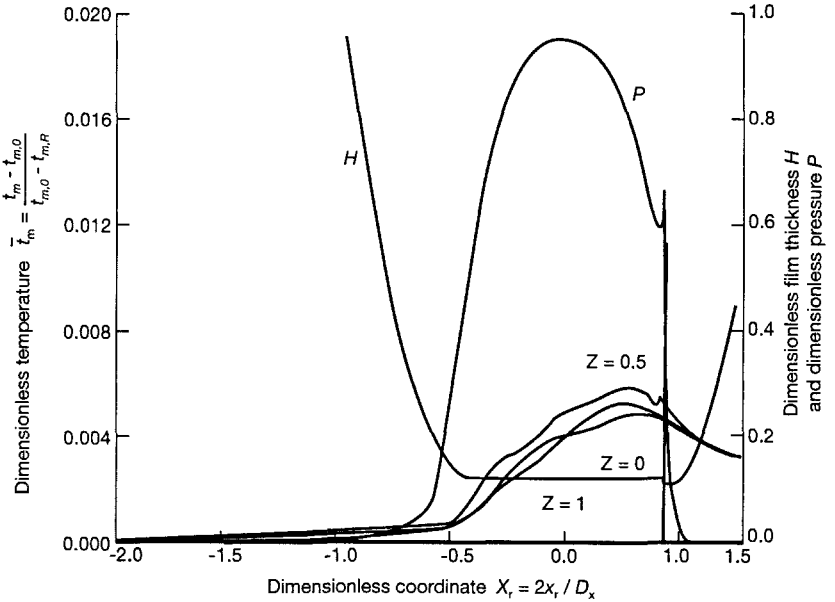

(c)

Figure 23.11: *Continued.*

Copyright © 2004 Marcel Dekker, Inc.

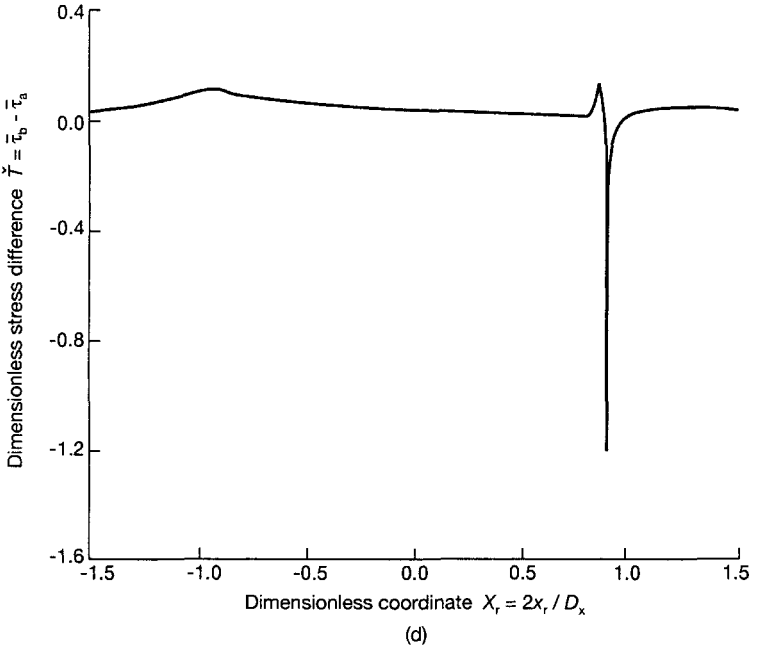

Figure 23.11: *Concluded.*

simultaneously. Using a conservative energy equation avoided the need for a delicate numerical procedure to obtain a converged solution for a thermal EHL conjunction that includes strong reverse flows. Applying a two-dimensional heat flow model validated the evaluation of the solid-liquid interface temperatures for an EHL conjunction with a near-stationary solid surface. Film collapse due to a high slide/roll ratio, which is predicted by the isothermal circular non-Newtonian fluid model, does not seem to happen when the thermal effect is considered. Two separate streams flowing in opposite directions may develop instead.

The strong effect of temperature rises on the traction developed in an EHL conjunction was confirmed. When the thermal effect is considered at a high slide/roll ratio, the friction coefficient may be only one-half of that predicted by the isothermal model.

23.4 Problems

23.1 The moving face of a parallel-surface slider bearing has a velocity of u_0 and a temperature of $t_{m,0}$, while the stationary surface, which is at a distance

Copyright © 2004 Marcel Dekker, Inc.

h, has a temperature $t_{m,1}$. The lubricant is pressure fed so that a uniform pressure gradient $(-g)$ is established in the direction of motion. If it is assumed that steady-state conditions exist, the bearing is of infinite width and the lubricant properties are invariant with temperature, show that the velocity profile across the film is parabolic. Also derive an expression for the temperature profile. Comment on the effect on energy dissipation and on the temperature profile if viscosity is taken to vary with temperature.

23.2 An incompressible, viscous fluid flows symmetrically in laminar flow along a circular-section tube of radius r_w. Flow is fully developed, and the velocity u at radius r is given by $u = 2v(1 - R^2)$, where v is the mean velocity and $R = r/r_w$.

The temperature profile in the fluid is fully developed, with no temperature gradient in the axial direction. The inner surface of the tube is maintained at a constant temperature. Show that the temperature t_m of the fluid at radius r is given by

$$t_m - t_{m,w} = \frac{\eta v^2}{K_f}\left(1 - R^4\right)$$

where

K_f = thermal conductivity of fluid
η = viscosity of fluid

Explain the importance of the energy equation in the fundamental design of the bearings.

References

Archard, J. F. (1958-59): The Temperature of Rubbing Surfaces. *Wear*, vol. 2, pp. 438-455.

Bair, S., and Winer. W. O. (1979): Shear Strength Measurements of Lubricants at High Pressure. *J. Lubr. Technol.*, vol. 101, pp. 251-257.

Barus, C. (1893): Isotherms, Isopiestics, and Isometrics Relative to Viscosity. *Am. J. Sci.*, vol. 45. pp. 87-96.

Blok, H. (1937): General Discussion on Lubrication. *Inst. of Mech. Eng.*, London. vol. 2, P. 222.

Cheng, H. S. (1965): A Refined Solution to the Thermal- Elastohydrodynamic Lubrication of Rolling and Sliding Cylinders. *ASLE Trans.*, vol. 8, pp. 397-410.

Cheng, H. S. (1967): Calculation of Elastohydrodynamic Film Thickness in High Speed Rolling and Sliding Contacts. Tech. Rep. MTI-67 TR24. Mechanical Technology Incorporated.

Conry, T. F. (1981): Thermal Effects on Traction in EHD Lubrication. *J. Lubr. Technol.*, vol. 103, pp. 533-538.

Copyright © 2004 Marcel Dekker, Inc.

Dowson, D., and Hudson, J.D., (1964): Thermohydrodynamic Analysis of the Infinite Slider Bearing, *Proc. I. Mech. E.*, v. 3, pp. 34-51.

Dowson, D., and Whitaker, A. V. (1965-1966): A Numerical Procedure for the Solution of the Elastohydrodynamic Problem of Rolling and Sliding Contacts Lubricated by a Newtonian Fluid. *Proc. Inst. Mech. Eng.*, London, vol. 180, no. 313, pp. 57-71.

Fillon, M., and Khonsari, M.M., (1996): Thermohydrodynamic Design Charts for Tilting Pad Journal Bearings, *J. Tribol.*, v. 118, pp. 232-238.

Gecim, B., and Winer. W. O. (1980): Lubricant Limiting Shear Stress Effect on EHD Film Thickness. *J. Lubr. Technol.*, vol. 102, pp. 213-221.

Ghosh, M. K., and Hamrock, B. J. (1985): Thermal Elastohydrodynamic Lubrication of Line Contracts. *ASLE Trans.*, vol. 28, no. 2, pp. 159-171.

Houpert, L. G., and Hamrock, B. J. (1986): Fast Approach for Calculating Film Thicknesses and Pressures in Elastohydrodynamically Lubricated Contacts at High Loads. *J. Tribol.*, vol. 108, pp. 411-420.

Hsiao, H. S., and Hamrock, B. J. (1992): A Complete Solution for Thermal-Elastohydrodynamic Lubrication of Line Contacts Using Circular Non-Newtonian Fluid Model. *J. Tribol.*, ASME paper 91-Trib-24.

Jacobson, B.O., (1970): On the Lubrication of Heavily Loaded Spherical Surfaces Considering Surface Deformation and Solidification of the Lubricant, *Acta Polytechnica Scandinavica*, Mech. Eng. Series No. 54.

Johnson, K. L. (1970): Regimes of Elastohydrodynamic Lubrication. *J. Mech. Eng. Sci.*. vol. 12, no. 1, pp. 9-16.

Khonsari, M.M., (1987): A Review of Thermal Effects in Hydrodynamic Bearings, *ASLE Trans.*, v. 30, pp. 19-20.

Khonsari, M.M., Jang, J.Y., and Fillon, M., (1996): On the Generalization of Thermohydrodynamic Analysis for Journal Bearings. *J. Tribol.*, v. 118, pp. 571-579.

Lee, R. T., and Hamrock. B. J. (1990): A Circular Non-Newtonian Fluid Model: Part 1-Used in Elastohydrodynamic Lubrication. *J. Tribol.*, vol. 112, pp. 486-496.

Okamura, H. (1982): A Contribution to the Numerical Analysis of Isothermal Elastohydrodynamic Lubrication, Tribology of Reciprocating Engines. *Proceedings of the Ninth Leeds-Lyon Symposium on Tribology.* Butterworths, Guilford, England, pp. 313-320.

Pinkus, O., and Wilcock, D.J., (1980): Thermal Effects in Fluid Film Bearings, *Proc. 6th Leeds-Lyon Symposium on Tribology*, I. Mech. E., London, pp. 3-23.

Pinkus, O., (1990) *Thermal Aspects of Fluid Film Tribology.* New York, ASME Press.

Richmond, J., Nilsson, O., and Sandberg, O. (1984): Thermal Properties of Some Lubricants Under High Pressure. *J. Appl. Phys.*, vol. 56, no. 7, pp. 2065-2067.

Roelands, C. J. A., Vlugter. J. G., and Waterman, H. I. (1963): The Viscosity-Temperature-Pressure Relationship of Lubricating Oils and Its Correlation

Copyright © 2004 Marcel Dekker, Inc.

With Chemical Constitution. *J. Basic Eng.*, pp. 601-610.

Rosenthal, D. (1946): The Theory of Moving Sources of Heat and Its Application to Metal Treatment. *ASME J.Tribology* pp. 849-866.

Sadeghi, F., and Dow, T. A. (1987): Thermal Effects in Rolling/Sliding Contacts: Part 2-Analysis of Thermal Effects in Fluid Film. *J. Tribol.*, vol. 109, pp. 512-518.

Shieh, J. A., and Hamrock, B. J. (1991): Film Collapse in EHL, and Micro-EHL. *J. Tribol.*, vol. 113, pp. 372-377.

Smith, F.W. (1958/59): Lubricant Behavior in Concentrated Contact Systems - The Castor Oil-Steel System, *Wear*, vol. 2, pp. 250-263.

Tsai, C. L. (1986): Welding Heat Transfer-Part I Conduction in Weldment. Class notes. Department of Welding Engineering, The Ohio State University.

Wang, S., Cusano, C., and Conry, T. F. (1991): Thermal Analysis of Elastohydrodynamic Lubrication of Line Contacts Using the Ree-Eyring Fluid Model. *J. Tribol.*, vol. 113, pp. 232-244.

Wang, S. H., and Zhang, H. H. (1987): Combined Effects of Thermal and Non-Newtonian Character of Lubricant on Pressure, Film Profile, Temperature Rise, and Shear Stress in EHL. *J. Tribol.*, vol. 109, pp. 666-670.

Wilson, W.R.D., (1998): A Framework for Thermohydrodynamic Lubrication Analysis. *J. Tribol.*, v. 120, pp. 399-405.

Wilson. W. R. D., and Huang, X. B. (1990): Discussion in a Circular Non-Newtonian Fluid Model: Part 1-Used in Elastohydrodynamic Lubrication. Lee, R. T., and Hamrock, B. J. *J. Tribol.*. vol. 112, pp. 486-496.

Zhu, D., and Wen, S. Z. (1984): A Full Solution for the Thermalelastohydrodynamic Problem in Elliptical Contacts. *J. Tribol.*, vol. 106, pp. 246-254.

Copyright © 2004 Marcel Dekker, Inc.